Journal of Fluids and Structures (2002) **16**(6), 691–713
doi:10.1006/jfls.447. available online at http://www.idealibrary.com on IDEAL®

LINEAR AND NONLINEAR DYNAMICS OF CANTILEVERED CYLINDERS IN AXIAL FLOW. PART 1: PHYSICAL DYNAMICS

M.P. Païdoussis, E. Grinevich, D. Adamovic† and C. Semler

Department of Mechanical Engineering, McGill University
Montreal, Québec, Canada H3A 2K6

(Received 25 January 2001; and in final form 27 August 2001)

This paper is the first in a three-part study of the dynamics of cantilevered cylinders in axial flow. After an extensive literature review, the *physical dynamics* of the system is examined; specifically (a) the experimental behaviour of elastomer cylinders in water flow, and (b) the energy transfer mechanisms, discussed from a work–energy perspective without solving the equations of motion. In general, the system loses stability by divergence and, as the flow velocity is increased, it is subject to second- and third-mode flutter, provided that the free end is well-streamlined; if, however, the free end is blunt, these instabilities do not occur. Oscillations are generally three-dimensional (orbital). The experimental observations are in good qualitative agreement with those expected from the energy transfer analysis, and in reasonably good quantitative agreement with solutions of the linearized equation of motion (obtained from Part 3 of this study). For some shapes of the free-end, resonances are observed with a fairly constant Strouhal number. © 2002 Elsevier Science Ltd. All rights reserved.

1. INTRODUCTION

Understanding and prediction of the dynamics of cylinders in axial flow is of interest for the design and trouble-free operation of heat-exchanger tubes, nuclear fuel elements, control rods and monitoring tubes, towed flexible cylinders for water transportation, towed acoustic arrays for oil exploration, and high-speed trains; also, by analogy, for paper making and tape winding.

Historically, the first specific study was by Hawthorne (1961) and was concerned with the stability of a long sausage-like towed container (a "Dracone"), conceived for the transport of oil by sea, following the Suez crisis of 1956; later, it found its greatest use in transporting fresh water to arid Greek islands from the mainland, and other, lighter than sea-water cargo elsewhere.

This analysis was extended and generalized for cylinders with any boundary conditions, e.g. simply supported, cantilevered and so on, and was supported by experiments, by Païdoussis (1966*a*, *b*). An error in the manner of incorporating the viscous forces into the equation of motion was corrected by Païdoussis (1973) and the theory further extended to deal with cases of confined flow; this correction, however, came too late to prevent the use

†Presently at CAE Electronics Ltd, 8585 chemin de la Côte-de-Liesse, Saint-Laurent, QC, Canada H4L 4X4.

0889-9746/02/060691 + 21 $35.00/0 © 2002 Elsevier Science Ltd. All rights reserved.

of the original formulation by others, e.g., Ortloff & Ives (1969). The divergence (buckling) critical flow velocity for a pinned-free cylinder has been determined analytically by Triantafyllou & Chryssostomidis (1984). The dynamics of long, very slender cylinders—modelled as strings, rather than beams—has been studied by Triantafyllou & Chryssostomidis (1985), among others.

This work was later pursued further to study the dynamics of clustered cylinders in axial flow (Chen 1975; Païdoussis 1979; Gagnon & Païdoussis 1994*a*, *b*), both because of its inherent interest and for application to tube-in-shell type heat exchangers and nuclear reactors. Also, additional extensions have been made, to deal with the dynamics in highly confined annular flow—see, e.g. Païdoussis *et al.* (1990) and Mateescu *et al.* (1994*a*, *b*, 1996).

The dynamics of towed cylinders is of interest, not only for the Dracone problem, but also for the towed "arrays" ("seismic arrays" or "acoustic streamers") used in oil exploration. Extremely long (kilometer-long) arrays of several parallel cylinders, housing sonar sensors, are towed on the sea surface or sufficiently submerged to avoid wave-induced motions. The sensors pick up acoustic signals directed at and reflected from the sea-bed strata. Properly analysed, these signals can reveal the geological make-up of the strata, and hence the existence of oil or gas. Apart from Hawthorne's original work, studies on towed systems were made by Païdoussis (1968, 1970),[1] Païdoussis & Yu (1976), Dowling (1988*a*, *b*), Triantafyllou & Chryssostomidis (1989), and many others. Other variants of the system have also been studied, e.g., the dynamics of tapered (conical) cylinders, articulated cylinders, and so on. For a more complete survey of the topic, the interested reader is referred to Païdoussis (2002).

The dynamics of cylinders in axial flow is dynamically similar to that of axially moving one-dimensional structures in quiescent fluid, such as paper "web" in paper-making, and travelling chains, bands and tapes—see, e.g., Mote (1968, 1972), Pramila (1986, 1987), Bejan (1982), Wickert & Mote (1990), Chang & Moretti (2000). The dynamics of this system is also closely related to that of pipes conveying fluid—see, e.g., Païdoussis (1998). This analogy will be used extensively in what follows.

The fluid forces exerted on a cylinder in axial flow may be viewed as being made up, principally, of inviscid fluid-dynamic forces, obtainable via slender body or three-dimensional potential flow theory. The slender-body approximation for the simplest possible system, yields the following equation of motion:

$$EI(\partial^4 y/\partial x^4) + M\,U^2(\partial^2 y/\partial x^2) + 2M\,U(\partial^2 y/\partial x \partial t) + F_v + (M+m)(\partial^2 y/\partial t^2) = 0, \quad (1)$$

where EI is the flexural rigidity and m the mass per unit length of the cylinder, U the flow velocity, y the lateral deflection, x the axial coordinate and t is the time; M is the virtual (or "added") mass of the fluid per unit length, which for unconfined flow is equal to the displaced mass of the fluid ($M = \rho A$, where A is the cross-sectional area of the cylinder). It is noted that in addition to the inviscid forces, there are coupled lateral and axial viscous forces due to surface traction exerted on the surface of the cylinder, represented by F_v in equation (1)—see equation (2) here and Part 2 of this study (Lopes *et al.* 2002); in contrast to internal flow, these are not cancelled by pressure-drop-related forces, since the pressure drop in the external flow is generally unrelated to the frictional forces on the cylinder (controlled by the boundary layer about it). If one puts $F_v = 0$ and reinterprets M as the mass per unit length of the fluid conveyed, equation (1) becomes that of the fluid-conveying pipe (Païdoussis 1998).

[1] With the aforementioned error in the viscous terms, and with it corrected, respectively.

It is not surprising therefore, that the dynamics of this system is similar, but not identical to that of the fluid-conveying pipe. Indeed, the differences in the dynamical behaviour between the internal and external flow systems are among the principal motivations for this work. Thus, according to linear theory, cylinders with both ends supported lose stability by divergence and at higher flow velocities by coupled-mode flutter. This dynamical behaviour is identical to that predicted for pipes conveying fluid, with the following important differences: (i) it has been shown by nonlinear theory (Holmes 1977, 1978) that coupled-mode flutter is impossible for pipes conveying fluid and, indeed, has never been observed in experiments, and (ii) post-divergence coupled mode flutter has been observed experimentally for cylinders in axial flow (Païdoussis 1966*b*). What is responsible for this important difference?

Cylinders supported only at the upstream end, e.g., cantilevered ones, generally lose stability by divergence and then, at higher flow velocities by single-mode flutter—as predicted by linear theory and observed in experiments. This behaviour is strongly dependent on the shape of the free end; indeed, the dynamics is as just described, provided the free end is fairly well streamlined. If the free end is blunt, however, neither divergence nor flutter occur; yet, the analogy to the internal flow system, superficially at least, is closest for the blunt-ended cylinder. Hence, again, the question arises as to how, as well as why, divergence can occur for the cylinder-in-flow system but not for the pipe-conveying fluid (Païdoussis 1998).

It is evident from the foregoing that there are sufficient practical applications to motivate the considerable effort devoted to this topic. It is fair to say, however, that a large component of this research has been curiosity-driven (Païdoussis 1993). In fact, the set of questions that have been posed when comparing the internal- and external-flow problems is of purely fundamental rather than practical interest.

Most of the work just cited on the topic under consideration concentrates on the linear dynamics of cylinders in axial flow. This three-part study represents perhaps the first attempt to consider the nonlinear dynamics of the system, and to present a cogent linear–nonlinear picture of the stability of the system, supported by a new series of experiments. Part 1, this paper, deals with the *physical dynamics* of the system, namely (i) the experimental observations of the dynamical behaviour, and (ii) the mechanisms of energy transfer, particularly concerned with flow-induced instabilities. Part 2 (Lopes *et al.* 2002) is entirely devoted to the equations of motion and discussion of methods of analysis. Part 3 (Semler *et al.* 2002) gives most of the theoretical results, linear and nonlinear, and the bulk of the comparison with theory.

2. EXPERIMENTS

2.1. The Apparatus

Experiments were conducted at two different times, in different locations, and with different apparatus.

The first set of experiments were conducted in the 1960s at the Chalk River Nuclear Laboratories of Atomic Energy of Canada (AECL). They are well-described in Païdoussis (1966*b*), and hence only the scantiest of description of the apparatus needs be given here. In these experiments, the flexible cylinders were mounted horizontally, in the horizontal test-section of a water-circulating rig. Most of the cylinders were manufactured by casting liquid silicone rubber in specially made moulds and vulcanized at room temperature, in the manner described in Païdoussis (1998, Appendix D). In most cases, the cylinders integrally

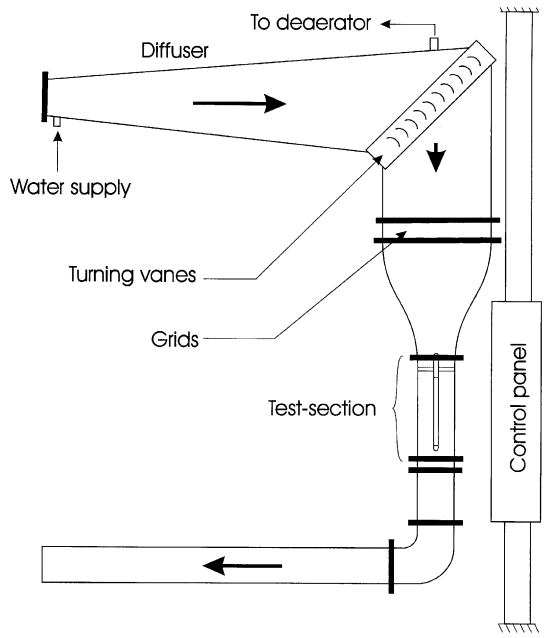

Figure 1. Diagrammatic view of part of the water tunnel used in the McGill experiments, showing the vertical test-section, with a flexible cantilevered cylinder mounted in it.

contained a thin blade (metal strip). The cylinder was mounted in the test-section such that the blade was in a vertical plane, thus ensuring that (i) the cylinder is horizontal at equilibrium (preventing sag, positive or negative), even for cylinder densities higher (typically) or lower (unusually, in the case of hollow cylinders) than that of water, and (ii) the oscillation takes place in a horizontal plane. Typical parameters for the cylinders used are: diameter $D = 16{\cdot}6\,\text{mm}$, length $L = 390\,\text{mm}$, flexural rigidity $EI = 6{\cdot}39 \times 10^{-3}\,\text{N m}^2$, mass per unit length $m = 0{\cdot}25\,\text{kg/m}$. Generally, a streamlined, ogival[2] rigid "end-piece", of the same density as the cylinder, was glued at the free end of the cylinder; it could be unglued and replaced by another, of different shape. Here, only some of the results from this set of experiments will be presented, for completeness, since some types of experiments were not repeated in the later set.

The second set of experiments were conducted in 1999–2000 at McGill University. The test-section was vertical, in a water tunnel shown diagrammatically in Figure 1. The flexible cylinder was mounted vertical, as shown in Figure 2. The cylinders were fabricated in basically the same manner; in this case, however, no central metal strip was embedded in the cylinder in most cases, as it was no longer essential. The test-section was larger than in the previous tests (test-section diameter $D_{\text{ch}} = 203\,\text{mm}$), and so were the cylinders (typically: $D = 25{\cdot}4\,\text{mm}$, $L = 520\,\text{mm}$, $m = 0{\cdot}577\,\text{kg/m}$, $EI = 5{\cdot}59 \times 10^{-2}\,\text{N m}^2$).

In both sets of experiments, flow straighteners, screens, and in the McGill experiments a large flow-area reduction, were utilized to ensure an axial, uniform flow stream in the test-section. Fluidelastic instabilities occurred at flow velocities for which the flow was turbulent (the Reynolds number based on the cylinder diameter was $\geq 5 \times 10^4$), and

[2]Ogive- or projectile-shaped.

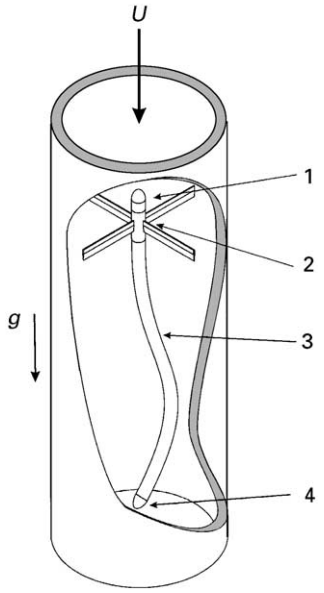

Figure 2. Schematic of the test-section, showing a flexible cylinder mounted in it: (1) fixed ogival upstream end; (2) cruciform support made up of symmetric-airfoil blades; (3) flexible cylinder; (4) ogival end-piece at the free end.

hence the velocity profile in the central part of the test-section may be assumed to be flat. In the McGill experiments, the turbulence intensity in the empty test-section was 0.5% or less.

In the experiments, the dynamics of the system was monitored, visually in the case of the AECL experiments (apart from measuring flow velocities, frequencies of motion, and such), and with the aid of a noncontacting optical motion-follower in the McGill tests, the output of which could be stored on a digital oscilloscope and analyzed with an FFT signal analyzer.

In each experiment the flow velocity was increased gradually from naught, and at each step the dynamical state of the system was recorded.

2.2. General Dynamical Behaviour

2.2.1. *Cylinders fitted with a metal strip: planar motions*

At small flow velocities, free motions were damped by the flow: small turbulence-induced disturbances were damped quickly, increasingly so with increased flow velocity. At sufficiently high flow velocities, however, the system became unstable provided that (i) the free end tapered smoothly, and (ii) the cylinder was not too long. If these conditions were met, as the flow velocity increased, the system first buckled [Figure 3(a)] and then spontaneously developed second-mode flutter [Figure 3(b)]. At still higher flow velocities, third-mode flutter was observed, followed, though rarely with the limited flow available, by fourth-mode flutter. In the course of flutter, the free end sloped backward to the direction of its motion for the greater part of the cycle. This "dragging" motion is necessary to allow the cylinder to absorb energy from the fluid stream; see Figure 3(b) and Section 3.2; cf. the form of a fluttering pipe conveying fluid (Païdoussis 1998, Section 3.2.2).

Divergence developed slowly with increasing flow velocity, and it was not always possible to determine the point of neutral stability accurately. The point of onset of oscillatory instabilities, on the other hand, was usually very clearly defined. According to linearized theory, once the threshold of instability is crossed, the amplitude of motion should increase without limit. In fact, because of nonlinear effects, the maximum displacement in buckling and the amplitude of amplified oscillations were limited to usually one to three cylinder diameters. If the flow velocity was reduced below the point where oscillatory instability first occurred, the oscillation persisted with reduced amplitude; this also is an attribute of nonlinear behaviour.

Transition from divergence to second-mode flutter involved a gradual return of the cylinder to its straight equilibrium configuration, before further increase in the flow velocity resulted in unstable oscillation.[3] Increasing the flow velocity further at this point caused the amplitude and frequency of oscillation to increase, until the motion became erratic and the frequency was gradually reduced to nil; the cylinder then appeared to be buckled in its second mode. At this point, a small increase in the velocity precipitated third-mode flutter of the system.

These general observations were the same for both the earlier experiments with motions in a horizontal plane and the more recent ones with vertically hanging cylinders, provided that motions were *planar*. Collectively, these observations show that the general behaviour of the system with increasing flow velocity is in substantial qualitative agreement with theory.

A ciné-film and video have been made, showing the development of these instabilities. One remarkable sequence that was fortuitously captured on film occurred because flutter on one occasion was large enough to cause impact of the free end on the flow-containing channel. Eventually, while the camera was running, the glued end-piece came off and was swept downstream, whereupon the cylinder was instantly stabilized and remained straight thereafter! This is a graphic illustration that a system with a blunt end is stable.

2.2.2. *Cylinders without metal strip: 3-D motions*

If the cylinder did not contain a metal strip which effectively limited its motion to one plane only, instability developed in that particular plane and, in the case of divergence, remained in this plane. Amplified oscillation, on the other hand, soon degenerated into a three-dimensional motion, in which the plane of oscillation rotated slowly while the free end described a quasi-circular path; i.e., a kind of whirling, "orbital" motion developed, but generally with nonstationary nodes. This was the case in most of the McGill experiments, except for a few that were made with a cylinder fitted with a metal strip.

Figure 4 shows photos of the instantaneous shape of the cylinder in divergence, second- and third-mode flutter in a typical case, for a cylinder fitted with a fairly well-streamlined end-piece. It is virtually impossible to discern the whirling character of the flutter from 2-D pictures, but this is easier to see in the video which has been made for the dynamics of a cylinder fitted with several different end-pieces.

Further experiments were conducted with a hollow cylinder fitted with a metal strip and mounted vertically, as well as with another similar cylinder without a metal strip. The dynamics of the two systems, with and without the metal strip, was essentially the same, despite motion being planar in one case and whirling in the other. Indeed, apart from this 2-D/3-D difference, the dynamics in the two cases was qualitatively quite similar in every way.

[3] In some cases with the cylinders hanging vertically, however, the cylinder retained a degree of bowing at the onset of flutter.

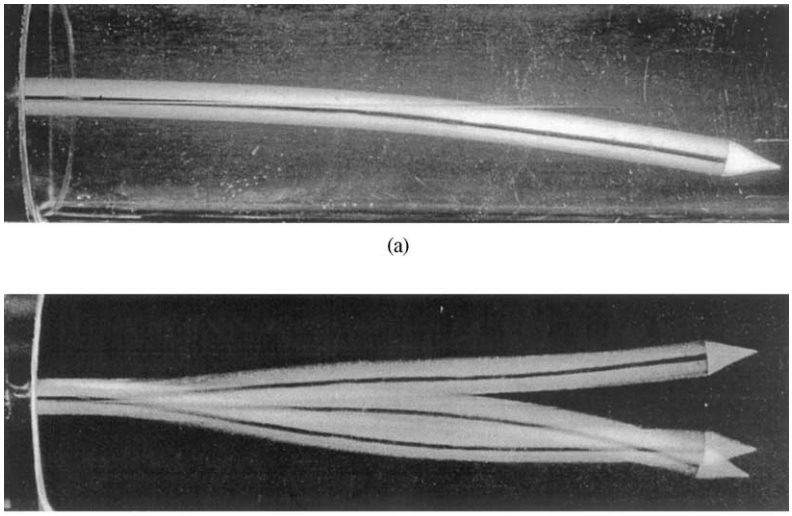

Figure 3. Photographs of a flexible cantilevered cylinder (a) in divergence, and (b) undergoing second-mode flutter. In this case the cylinder contains a vertical metal strip, and the motion is in a horizontal plane.

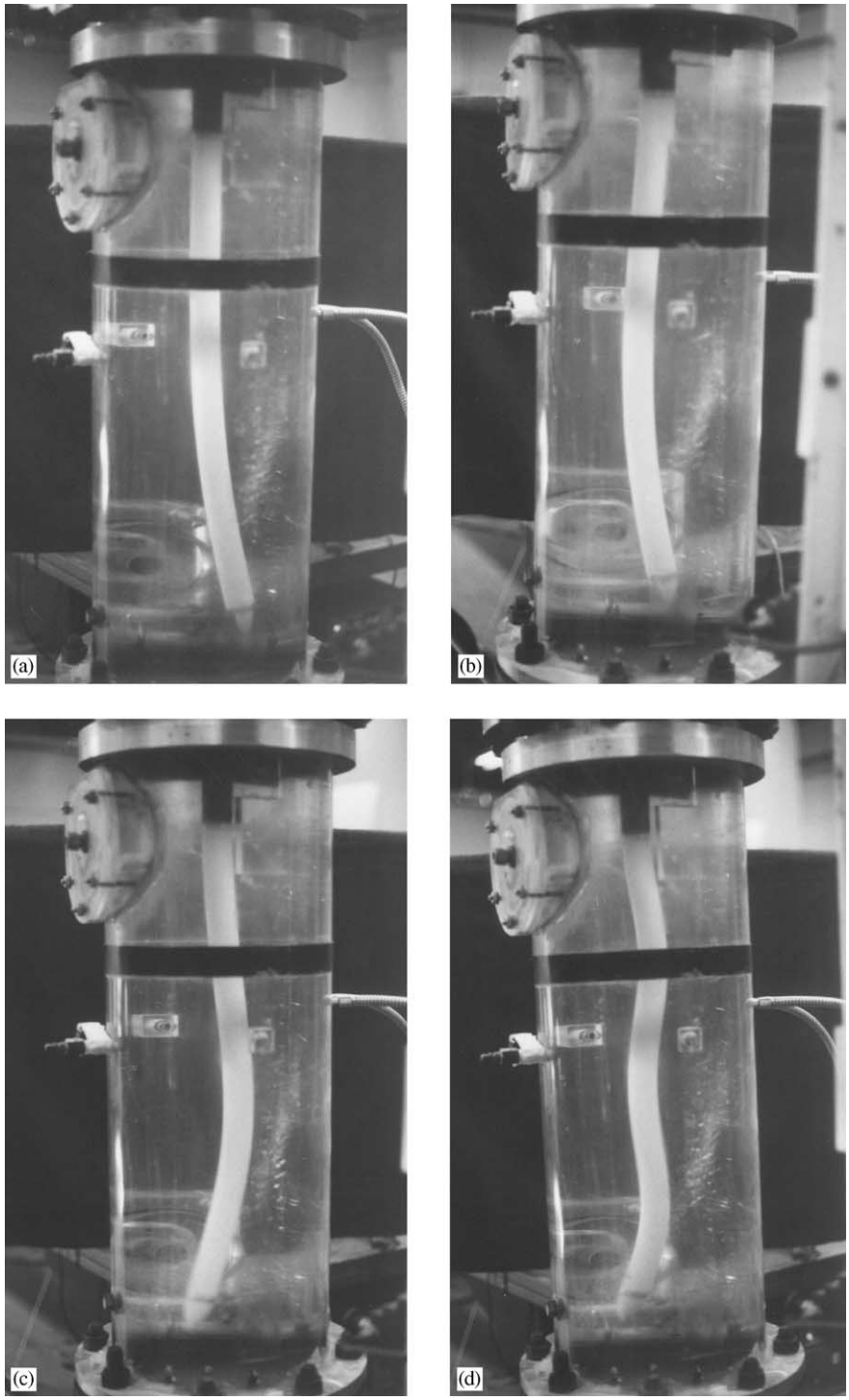

Figure 4. Photographs of a vertical flexible cylinder in divergence at relatively low flow velocity, (b) divergence at relatively high flow velocity, as the threshold of flutter is approached; (c) in second-mode 3-D flutter; (d) in third-mode 3-D flutter.

Nevertheless, there were *some* differences in the dynamics of cylinders in 2-D motion (horizontal cylinder) or 3-D motion (vertical cylinders), specifically in the transition from one instability to another; e.g., in the latter, transition from second- to third-mode flutter was not usually preceded by a quasi-stationary (vanishing frequency) state, but it involved erratic, perhaps quasi-periodic, oscillations—to be discussed further in Part 3.

Additional experiments were conducted with a vertical blade-fitted cylinder, with three holes drilled in the ogival end-piece, such that some of the fluid could go transversely through, rather than around the end-piece, as the cylinder oscillated. Two such perforated end-pieces were used, differing only in the pattern of the drilled holes. With one end-piece, both divergence and flutter were eliminated in this way; with another, only divergence was, while flutter still occurred, but at higher flow velocity.

Similar observations were made with a *cylinder pinned at the upstream end* and free at the other (Païdoussis 1966*b*). The specific gravity of this cylinder was very nearly that of water, so that gravity and buoyancy forces balanced almost exactly, making experiments in the horizontal plane feasible. The various instabilities occurred at lower flow velocities than for a similar cylinder with the upstream end clamped, and it was easily possible to observe fourth-mode flutter.

2.3. Quantitative Aspects

Several series of experiments have been conducted, in which some parameters were varied systematically, namely the shape of the free end, the mass ratio β, and the slenderness ratio ε—to be defined shortly. Some of the early experimental results have been presented in Païdoussis (1966*b*), where they were compared with the uncorrected theory (see Introduction). A portion of these were compared to the corrected theory in Païdoussis (1973), while some were left out. These latter, together with the newer experiments, are presented here.

Although comparison of experiment with theory to a large extent is done in Part 3 of this paper—especially the nonlinear aspects—it is more efficient to show the experimental results to be presented here *together with the theoretical results*. For this purpose, but also because it will be needed for Section 3, the linearized equation of motion is given here; for its derivation, see Part 2.

For a vertical cylinder of mass per unit length m, flexural rigidity EI, length L, diameter D, and cross-sectional area A, in unconfined flow parallel to the cylinder axis of density ρ and axial flow velocity U, the linearized equation of motion (Païdoussis 1973; Lopes *et al.* 2002) is

$$\begin{aligned}
&\left(E^*\frac{\partial}{\partial t}+E\right)I\frac{\partial^4 y}{\partial s^4}+\rho A\left(\frac{\partial}{\partial t}+U\frac{\partial}{\partial s}\right)^2 y\\
&-\left\{\left[\tfrac{1}{2}\rho\, D\, U^2\, C_T+(m-\rho A)g\right](L-x)+\tfrac{1}{2}\rho\, D^2\, U^2\, C_b\right\}\frac{\partial^2 y}{\partial s^2}\\
&+\tfrac{1}{2}\rho\, D\, U\, C_N\left(\frac{\partial y}{\partial t}+U\frac{\partial y}{\partial s}\right)+\tfrac{1}{2}\rho\, D\, C_D\frac{\partial y}{\partial t}+(m-\rho A)g\frac{\partial y}{\partial s}+m\frac{\partial^2 y}{\partial t^2}=0.
\end{aligned}\tag{2}$$

In this equation, $\rho A \equiv M$ is the virtual (added) mass of the fluid per unit length, C_N and C_T are the frictional forces in the normal (transverse) and longitudinal directions, respectively, C_D is a linearized form drag coefficient[4] for transverse motions, C_b is the

[4] This coefficient is *dimensional*, with dimensions of velocity.

coefficient of base drag acting in the longitudinal direction at the free end of the cylinder, and E^* is the Kelvin–Voigt damping coefficient in the cylinder material; y is the transverse displacement, and s is the curvilinear coordinate along the cylinder centre-line.

The boundary conditions are: $y(0) = 0, (\partial y/\partial s)_{s=0} = 0$ and

$$-EI\frac{\partial^3 y}{\partial s^3} - fMU\left(\frac{\partial y}{\partial t} + U\frac{\partial y}{\partial s}\right) + \tfrac{1}{2}\rho\, D\, U\, C_f\left(\frac{\partial y}{\partial t} + U\frac{\partial y}{\partial s}\right)\bar{s}_e + \left[fMU\left(\frac{\partial^2 y}{\partial t^2} + U\frac{\partial^2 y}{\partial s\partial t}\right) + m\frac{\partial^2 y}{\partial t^2} + (m-\rho A)g\frac{\partial y}{\partial s}\right]s_e = 0, \tag{3a}$$

$$\frac{\partial^2 y}{\partial s^2} = 0 \tag{3b}$$

at $s = L$, where

$$s_e = \frac{1}{A}\int_{L-l}^{L} A(s)\,\mathrm{d}s, \quad \bar{s}_e = \frac{1}{D}\int_{L-l}^{L} D(s)\,\mathrm{d}s \tag{4}$$

and where it is understood that $A \equiv A|_{L-l}, D \equiv D|_{L-l}, m = m|_{L-l}, M = \rho A$. In equation (3a), the parameter f, normally $f < 1$, is a measure of departure from the ideal lift that would arise if the end of the cylinder were perfectly streamlined, and there were no flow separation over it—in which case $f = 1$. Thus, $f \to 1$ corresponds to a well-streamlined end-piece, while $f \to 0$ to a blunt end; refer to Section 6 of Part 2. Of course, in addition to f diminishing, as the end becomes blunter, C_b would be expected to increase correspondingly.

These equations are rendered dimensionless by defining $\xi = s/L$, $\eta = y/L, \tau = \{EI/(m+\rho A)\}^{1/2} t/L^2$ and

$$\mathscr{U} = \left(\frac{\rho A}{EI}\right)^{1/2} UL, \quad \beta = \frac{\rho A}{\rho A + m}, \quad \gamma = \frac{(m-\rho A)gL^3}{EI}, \quad \varepsilon = \frac{L}{D},$$

$$\alpha = \left[\frac{I}{E(\rho A + m)}\right]^{1/2}\frac{E^*}{L^2}, \quad c_N = \frac{4}{\pi}C_N, \quad c_T = \frac{4}{\pi}C_T, \quad c_b = \frac{4}{\pi}C_b,$$

$$c_d = \left(\frac{M}{EI}\right)^{1/2} L\, C_D, \quad \chi_e = \frac{s_e}{L}, \quad \bar{\chi}_e = \frac{\bar{s}_e}{L}. \tag{5}$$

The dimensionless linearized equation of motion is given in Part 2 as equation (55), and the boundary conditions at $\xi = 1$ in equations (67).

In what follows, in this paper, we usually take $\alpha = 0$, $c_d = 0$, and often $c_N = c_T = c_f$.

2.3.1. *The critical flow velocities*

Figure 5 shows the average dimensionless tip displacement, $\bar{\eta}^*(1) = \bar{y}(L)/D$, of a cylinder with two different ogival ends (both reasonably well streamlined) as the dimensionless flow velocity $\mathscr{U}$ increases. Ideally, the displacement should be zero, from $\mathscr{U} = 0$ to the critical flow velocity for divergence, $\mathscr{U}_{cd}$, when the amplitude should increase sharply, with infinite slope, $\bar{\eta}^*(1)/\mathscr{U} = \tan^{-1}(\frac{1}{2}\pi)$. In reality, however, one obtains nonzero $\bar{\eta}^*(1)$ for all $\mathscr{U} > 0$. In fact, one can discern two zones in the figure: (i) for $\mathscr{U} < 2$ approximately, the rate of increase of $\bar{\eta}^*(1)$ with $\mathscr{U}$ is moderate, and this may be identified with the growth (exaggeration) of initial imperfections, both geometric and structural; (ii) for $2 < \mathscr{U} < 2{\cdot}5$ approximately, there is a steeper rate of increase of $\bar{\eta}^*(1)$ with $\mathscr{U}$, and this may be identified with the development of divergence. The results in Figure 5 are relatively

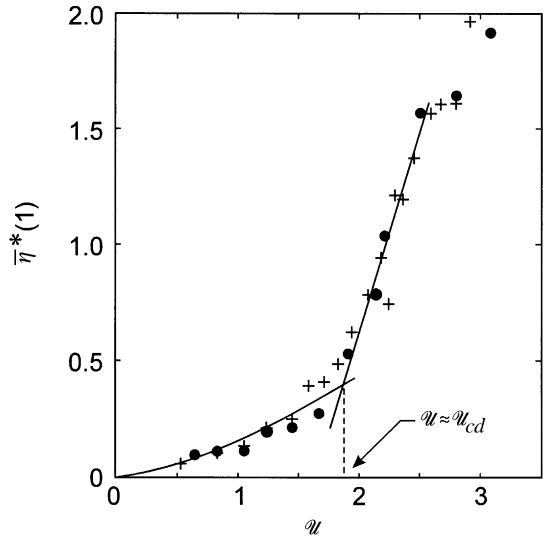

Figure 5. The dimensionless mean displacement of the free-end tip of the cylinder, $\bar{\eta}^*(1) = \bar{y}(L)/D$, as a function of increasing dimensionless flow velocity, $\mathscr{U}$, showing the development of divergence. The dots and crosses represent experiments with two different but similar ogival ends.

"clean", whereas in other runs they are more ambiguous. Consequently, the rougher but more reliable criterion of $\bar{\eta}^*(1)$ surpassing an arbitrary value, typically 1·0, was used alternatively for the threshold of divergence. Finally, for $\mathscr{U} > 2{\cdot}5$ approximately, the buckled shape of the cylinder begins to become S-shaped, indicating the increasing contribution of the second beam mode in the in-flow first-mode shape; the rate of increase of $\bar{\eta}^*(1)$ with $\mathscr{U}$ becomes smaller; in fact, for high enough $\mathscr{U}$, a diminishing $\bar{\eta}^*(1)$ may result.

By monitoring the r.m.s. amplitude of vibration with increasing flow velocity, one can easily pin-point the onset of flutter, as shown in Figure 6. In these results, the noncontacting sensor was trained at $\xi \equiv x/L = 0{\cdot}39$. It is seen that there is little doubt in this case as to where the threshold of flutter is. The reduction of amplitude, after a high of $0{\cdot}37D$ is reached, reflects gradual changes in modal shape with flow velocity.

Figure 7 shows the PSDs of the vibration of the cylinder, with the same sensor trained at the same location. Figure 7(a,b) shows typical spectra of the turbulence-induced vibration for pre-divergence flow velocities, $\mathscr{U} < \mathscr{U}_{cd}$. The dominant vibration frequencies at $f_1 \simeq 0{\cdot}6$, $f_2 \simeq 2{\cdot}9$ and $f_3 \simeq 8{\cdot}0$ Hz may be identified with the first-, second- and third-mode eigenfrequencies of the system. Here, it should be noted that the eigenfrequencies vary with $\mathscr{U}$, but they remain identifiable, more or less at the values cited.

In Figure 7(a), and also 7(b) if the location of sensing the vibration is taken into account, first-mode vibration at f_1 dominates. This is not necessarily so for post-divergence flow velocities, $\mathscr{U} > \mathscr{U}_{cd}$, as shown in Figure 7(c,d), where f_2 becomes more prominent. Nevertheless, a component at f_1 remains identifiable in most cases. This suggests that, in its buckled state, the cylinder has nonvanishing first-mode frequency, i.e. nonzero stiffness. This statement, heretical from a linear dynamics perspective, is perfectly reasonable in nonlinear terms.

Once second-mode flutter develops, at $\mathscr{U} = \mathscr{U}_{cf2}$, f_2 is clearly dominant, as shown in Figure 7(e). Similarly, once third-mode flutter is established at $\mathscr{U} = \mathscr{U}_{cf3}$, the dominant frequency is f_3, as seen in Figure 7(f).

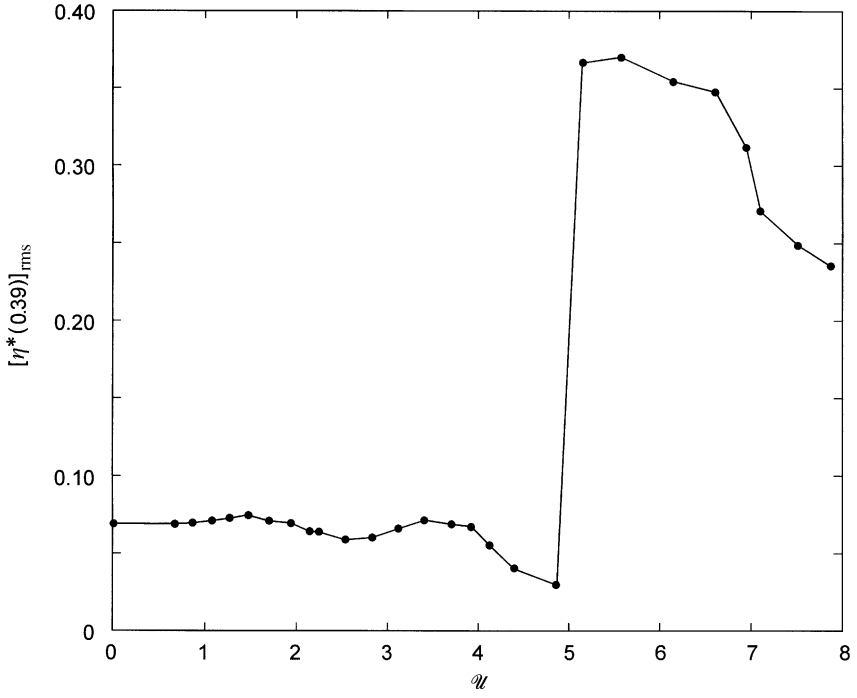

Figure 6. The r.m.s. amplitude of vibration at $\xi = 0{\cdot}39$, $[\eta^*(0{\cdot}39)]_{\text{r.m.s}}$, versus the dimensionless flow velocity $\mathscr{U}$, showing the onset of second-mode flutter.

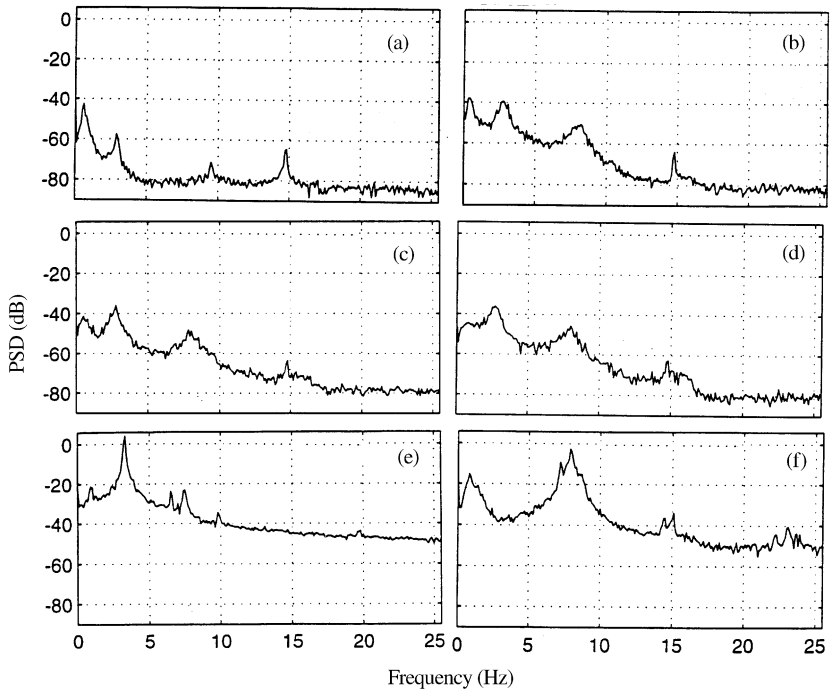

Figure 7. PSDs of vibration at $\xi = 0{\cdot}39$: (a,b) at pre-divergence flow velocities; (c,d) at post-divergence flow velocities; (e) in the course of second-mode flutter; (f) in the course of third-mode flutter. (a) $U = 0{\cdot}34\,\text{m/s}$ ($\mathscr{U} = 0{\cdot}53$); (b) $U = 1{\cdot}34\,\text{m/s}$ ($\mathscr{U} = 2{\cdot}10$); (c) $U = 1{\cdot}66\,\text{m/s}$ ($\mathscr{U} = 2{\cdot}61$); (d) $U = 2{\cdot}01\,\text{m/s}$ ($\mathscr{U} = 3{\cdot}16$); (e) $U = 3{\cdot}37\,\text{m/s}$ ($\mathscr{U} = 5{\cdot}29$); (f) $U = 4{\cdot}50\,\text{m/s}$ ($\mathscr{U} = 7{\cdot}08$).

2.3.2. *Effect of free-end shape*

A number of tests were conducted in which a cylinder was successively fitted with several ogival end-pieces, ranging from well-streamlined to blunt shapes. At the end of each test, the end-piece was removed and a new one glued in its place. The sequence was repeated several times, partly to overcome the effect of misalignments and to check repeatability (Païdoussis 1966*b*).

The critical flow velocities for divergence, $\mathscr{U}_{cd}$, and flutter, $\mathscr{U}_{cf}$, are compared with theoretical values in Figure 8 for the horizontal system (the earlier set of experiments).[5] The results in each case cover a considerable range in $\mathscr{U}$, indicating that small misalignments may have considerable effect on stability; this is especially true for $\mathscr{U}_{cd}$, the determination of which involved an element of subjective judgement. The arrows indicate that the system remained stable up to the maximum flow velocity of about 6 m/s attainable with the apparatus, corresponding to $\mathscr{U} \simeq 14$. Under such circumstances, "stable" means that no distinct divergence or oscillation developed; nevertheless, there were damped, apparently random motions of irregular frequency and amplitude.

For an ideally slender end, $f \to 1$ and $c_b \to 0$; while for blunter ends, $f < 1$ and $c_b > 0$. According to theory, decreasing f stabilizes the system for divergence, while increasing c_b destabilizes it.[6] These conflicting effects may have contributed to the poor agreement between theory and experiment for divergence, since for the theoretical results $c_b = 1 - f$ was taken arbitrarily throughout. The main reasons, however, are (i) the sensitivity of $\mathscr{U}_{cd}$ to imperfections, and (ii) the lack of refinement in the analytical model. Nevertheless, it is clear that, for a sufficiently blunt end, no divergence occurs.

For flutter, theory predicts that decreasing f and increasing c_b both have a stabilizing effect, as observed. Qualitatively, agreement with theory is considerably better in this case. Again, for a sufficiently blunt end, flutter is neither observed nor predicted in this flow velocity range.

Similar experiments were conducted in the vertical system (recent experiments). The experimental results for $\mathscr{U}_{cd}, \mathscr{U}_{cf2}$ and $\mathscr{U}_{cf3}$ are compared with theory in Figure 9; theoretical results for $\mathscr{U}_{cd}$ and $\mathscr{U}_{cf2}$ only are shown, since the transition from second- to third-mode flutter is generally nonlinear, as discussed in Part 3. Once more, it is seen that if the shape of the end-piece is sufficiently blunt, the system remains stable to the maximum available flow velocity, in this case 4·9 m/s or $\mathscr{U} = 7{\cdot}7$. It is of interest that, within the range of experimental error, the fine detail of the end-piece shape does not have as strong an effect on stability as might have been expected.

The dynamical behaviour of the system with end-piece #92 was peculiar, and it is discussed further at the end of this subsection; it should be remarked here, however, that the observed flutter, shown as second-mode flutter in Figure 9, could well really be third-mode flutter. Some additional experiments were conducted with end-piece #92S, a shortened version of #92 in which the cylindrical part of the end-piece (~ 10 mm) was machined off. In this case, there was no divergence at all, but flutter still occurred at $\mathscr{U}_{cf} \simeq 7{\cdot}5$, approximately the same as for the longer end-piece.

Experiments were also conducted with shortened versions of end-pieces #35 and #90, but similar results as for the longer ones were obtained.

Some further experiments were conducted with one end-piece (#15 in Figure 9), the end of which was lopped off progressively more radically. The experimental results are given in Table 1, where it is seen that taking off a small amount (5 or 10 mm) results in a reduced

[5] See Section 6 of Part 2 on the quantitative determination of f.

[6] For instance, for a system $\varepsilon c_f = 0{\cdot}5$ and $f = 0{\cdot}8$, for divergence we find $\mathscr{U}_{cd} = 1{\cdot}93$ for $c_b = 0$; $\mathscr{U}_{cd} = 1{\cdot}75$ for $c_b = 1$; $\mathscr{U}_{cd} = 1{\cdot}65$ for $c_b = 2$. For flutter, however, $\mathscr{U}_{cf} = 7{\cdot}51$ for $c_b = 0$, and $\mathscr{U}_{cf} > 10$ for $c_b = 1$.

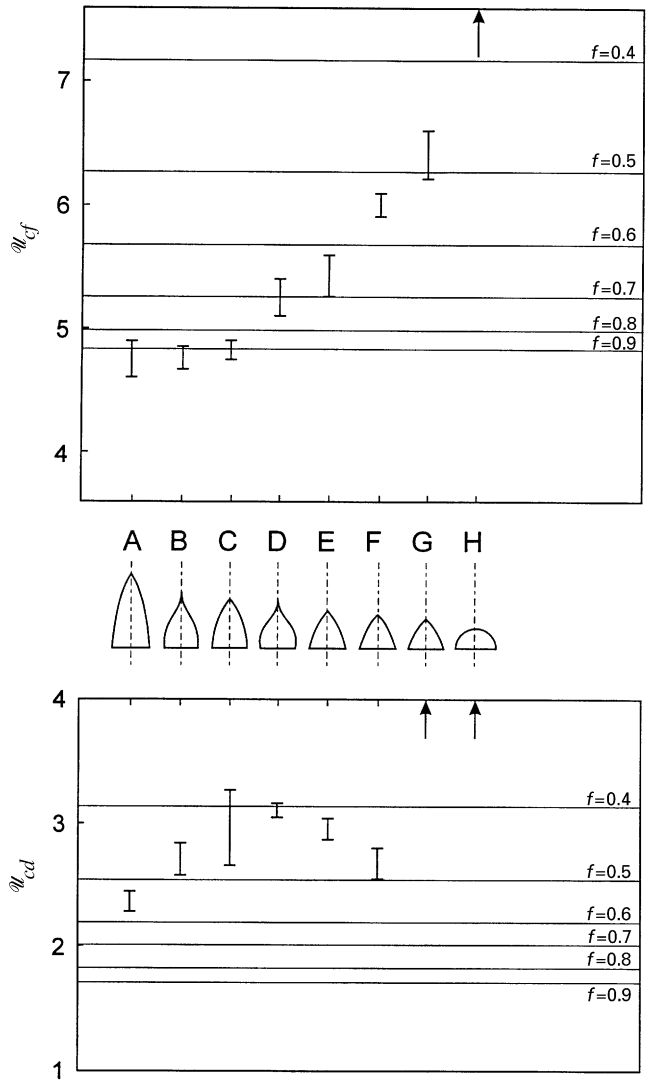

Figure 8. The critical flow velocities for divergence, $\mathscr{U}_{cd}$, and second-mode flutter, $\mathscr{U}_{cf2}$, as functions of the free-end shape for the horizontal system: I, experimental data; —, theoretical results for varying f and $c_b = 1 - f$ (other parameters: $\beta = 0{\cdot}46$, $\varepsilon c_N = \varepsilon c_T = 0{\cdot}25$, $\gamma = 0$, $c_d = 0$, $\chi_e = 0{\cdot}01$, $\bar{\chi}_e = 0$). The experimental results are from Païdoussis (1966*b*) and the theoretical ones with the present theory.

$\mathscr{U}_{cd}$; evidently this is associated with f being only slightly reduced but c_b becoming substantially higher as a result of the now partly flat end. The effect of a decreased f and higher c_b is stabilizing for flutter, as already remarked; hence, $\mathscr{U}_{cf}$ increases. Eventually, however, as the end is cut enough, the system is stabilized in both divergence ($\mathscr{U}_{cd}$) and second- and third-mode flutter ($\mathscr{U}_{cf2}$ and $\mathscr{U}_{cf3}$, respectively).

Finally, the unusual dynamical behaviour of the cylinder fitted with the #92 double-curvature end-piece should be commented upon. This system developed low-amplitude resonances before the onset of divergence, probably associated with vortex shedding at the free end. The cylinder oscillated in its second mode, with increasing amplitude as the flow velocity was increased, reaching a maximum and then gradually abating. This was

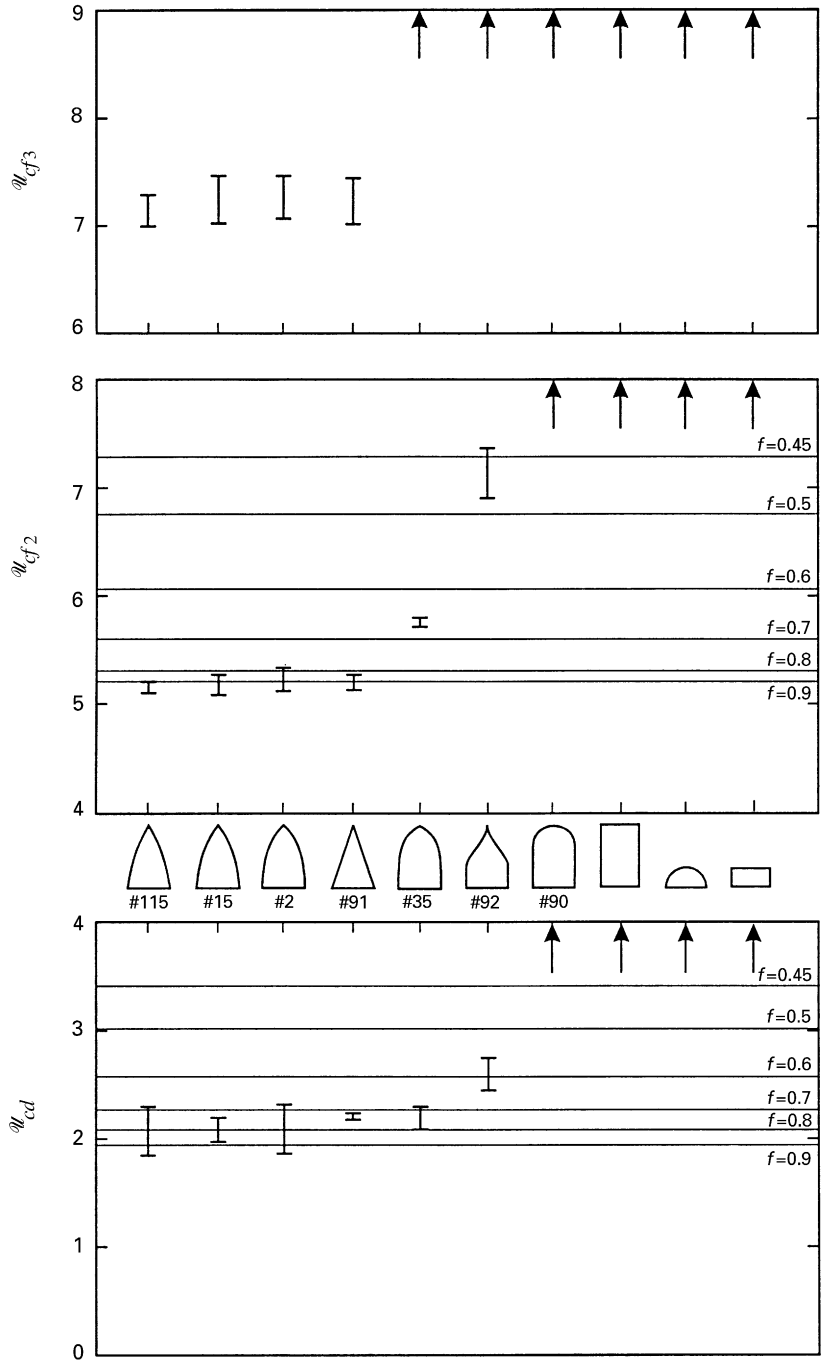

Figure 9. The critical flow velocities for divergence, $\mathscr{U}_{cd}$, and the second- and third-mode flutter, $\mathscr{U}_{cf2}$ and $\mathscr{U}_{cf3}$, respectively, as functions of the free-end shape for the more recent experiments with vertical cylinders (without metal strip): I, experimental data; —, theoretical results for varying f and $c_b = 1 - f$ (other parameters: $\beta = 0{\cdot}47$, $\varepsilon\, c_N = \varepsilon\, c_T = 0{\cdot}5$, $\gamma \equiv \gamma_C - \gamma_F = 1{\cdot}84, c_d = 0$, $\chi_e = 0{\cdot}00667$, $\bar{\chi}_e = 0{\cdot}00785$).

TABLE 1

Dimensionless critical flow velocities for a cantilevered cylinder with end-piece #15, the end of which was lopped off, progressively more. The asterisk denotes irregular flutter about the buckled state

End-shape	$\mathscr{U}_{cd}$	$\mathscr{U}_{cf2}$	$\mathscr{U}_{cf3}$
Intact (37 mm)	2·0–2·2	5·88	7·22
−5 mm lopped off	1·6–1·8	6·01	7·62
−10 mm lopped off	1·7–1·8	6·73*	7·86
−13 mm lopped off	1·8–2·0	—	—
−15 mm lopped off	2·2–2· 4	—	—
−20 mm lopped off	—	—	—

followed by third-mode vibration, behaving similarly, and then fourth-mode vibration. The vibration amplitude was $\sim 0{\cdot}5D$ for the second-mode resonance, and smaller for the higher ones. The resonance frequencies were $f_2 \simeq 3{\cdot}1$ Hz, $f_3 \simeq 8{\cdot}0$ Hz and $f_4 \simeq 15{\cdot}4$ Hz and the corresponding Strouhal numbers, $\mathrm{St} = fD/U$, were $\mathrm{St}_2 \simeq 0{\cdot}15$ and $\mathrm{St}_3 \simeq \mathrm{St}_4 \simeq 0{\cdot}17$. Similar behaviour was observed with the shortened version of #92 end-piece, #92S. The frequencies were similar, namely $f_2 \simeq 3{\cdot}0$ Hz, $f_3 \simeq 8{\cdot}1$ Hz and $f_3 \simeq 15{\cdot}5$ Hz, as were the Strouhal numbers: $\mathrm{St}_2 \simeq 0{\cdot}16$, $\mathrm{St}_3 \simeq 0{\cdot}18$ and $\mathrm{St}_4 \simeq 0{\cdot}18$ or 0· 19. Similar phenomena were observed in experiments with end-piece #90. However, this behaviour was unique to these two end-shapes.

2.3.3. *Effect of the mass ratio* β

Experiments in which β was varied were conducted in the horizontal system with two hollow cylinders successively filled with various substances, such as air, water, sand, lead shot and mercury. Some of these results are presented in Païdoussis (1973), and a fuller set in Païdoussis (2002). They will not be repeated here in the interests of brevity. Suffice it to say that the effect is substantial but not *very* strong; e.g. the values of $\mathscr{U}_{cf2}$ for the hollow and heaviest cylinder range between 3·8 and 5·8 for $\beta \simeq 0{\cdot}32$ and 0·60, respectively.

2.3.4. *Effect of surface roughness and slenderness*

Experiments were conducted with cylinders artificially roughened, in one case by rubbing with coarse sandpaper, and in another by gluing cotton thread helically around the cylinder (Païdoussis 1966*b*). It was found that a small stabilizing effect resulted, mainly on flutter: with the thread, $\mathscr{U}_{cf}$ was increased from 5·25 to 6·9–7·5. When rubber rings ($\frac{1}{2}$ in inside and $\frac{5}{8}$ in outside diameters) were fitted over the cylinder ($D = 0{\cdot}575$ in) at equally spaced intervals, no instability occurred at all.

Experiments were also conducted with one long cylinder ($\varepsilon = L/D = 46$), progressively reducing its slenderness by cutting pieces off the free end and then replacing the same end-piece. As seen in Table 2, when $\varepsilon > 24$ no divergence developed, while at $\varepsilon > 40$ there was no second-mode flutter, at least to the maximum attainable flow velocity. At $\varepsilon = 39{\cdot}5$ the amplitude and frequencies of the flutter were erratic, the latter vanishing occasionally while the cylinder retained an S-shape.

The explanation given at the time (1966) was that, as ε (and hence εc_f) increases, so does the stability of the system. This is undoubtedly so (see Part 3), and it agrees qualitatively with Triantafyllou & Chryssostomidis' (1984) finding that there exists a maximum εc_f ($\simeq 1{\cdot}4$) beyond which there is no divergence for $f < 0{\cdot}75$ approximately. However, to eliminate the instabilities altogether, the value of ε necessary would be much larger than

TABLE 2

The effect of ε on the critical flow velocities for divergence ($\mathscr{U}_{cd}$) and flutter ($\mathscr{U}_{cf}$); (Païdoussis 1966*b*)

ε	$\mathscr{U}_{cd}$	$\mathscr{U}_{cf}$
16·3	2·01	4·58
22·9	3·08	4·54
25·9	—	4·94
39·5	—	5·85
45	—	—

achieved in these experiments. A full explanation of this phenomenon goes beyond the theoretical model of Part 2, and should take into account the thickening of the boundary layer (when the length is large or the rings are present) and the resulting "insulating effect" of the cylinder from the mean flow, as discussed in Hannoyer & Païdoussis (1978).

3. MECHANISMS OF INSTABILITY

The objective here is to attempt physical explanations of the mechanisms of the observed divergence and flutter instabilities, by means of the equations of motion and the observed dynamical behaviour.

3.1. THE MECHANISM FOR DIVERGENCE

For cylinders with a free downstream end, more particularly cantilevered cylinders, the main destabilizing effect is associated with the tapered (ogival) free end. The destabilizing force is associated with the shear boundary condition (3a) which, after elimination of the time-dependent terms and taking $s = x$ for linear analysis, becomes

$$EI\frac{\mathrm{d}^3y}{\mathrm{d}x^3} + fMU^2\frac{\mathrm{d}y}{\mathrm{d}x} = 0. \tag{6}$$

Clearly, from the experiments, if $f = 0$, i.e. in the absence of a *tapered* end, divergence is impossible. An interesting connection between the term $fMU^2(\mathrm{d}y/\mathrm{d}x)$ and the lift on a low-aspect-ratio (slender) wing has been pointed out by Triantafyllou (1998).

To best appreciate this connection, it is useful to re-write the second term in (6) as M^*Uv, where $M^* = f\,M = f\,\rho A$ and $v = U(\mathrm{d}y/\mathrm{d}x)$. Furthermore, it is useful to recall how this term arises (see Part 2), namely via

$$\begin{aligned} &-f\int_{L-l}^{L}\left(\frac{\partial}{\partial t} + U\frac{\partial}{\partial x}\right)[M(x)v]\mathrm{d}x = -f\int_{L-l}^{L}U\frac{\mathrm{d}}{\mathrm{d}x}[\rho A(x)v]\,\mathrm{d}x \\ &= f\,\rho A\,Uv \equiv M^*Uv, \end{aligned} \tag{7}$$

in the last two versions of which it is understood that $A = A|_{L-l}$ and $M^* = M^*|_{L-l}$, corresponding to the cylindrical part of the body; to obtain this relationship, the fact that this is a static analysis has been invoked, as well as the assumption (Part 2) that v is constant over the tapered end. It is now clear from (7) that if $\mathrm{d}A/\mathrm{d}x = 0$, there would be no lift; i.e., in the absence of a tapered end-piece, there would be no lift and hence no divergence.

For a slender wing of chord c and span s, such that the aspect ratio $\mathrm{AR} \equiv s/c \ll 1$, the lift is $L = \frac{1}{2}\rho\,U^2AC_L$, in which $A = cs$. Taking $C_L \simeq (\mathrm{d}C_L/\mathrm{d}\psi)\psi \simeq (\mathrm{d}\,C_L/\mathrm{d}\psi)(v/U)$ and

recalling that $\mathrm{d}C_L/\mathrm{d}\psi \simeq \frac{1}{2}\pi(\mathrm{AR})$ from slender wing theory,[7] it is seen that $L = (\pi/4)\rho s^2 Uv = M^* Uv$, where M^* is the added mass of the wing. This is identical, therefore, to the expression for the cylinder-tail boundary condition obtained by slender-body theory. Furthermore, slender wing theory predicts (Katz & Plotkin 1991, Section 8.2.2) that there is lift only if the wing form is tapered (e.g., as it is for a delta wing). Hence, the similarity to the cylinder with a tapered end is quite close (Triantafyllou 1998).

A special set of calculations have been conducted for the cylinder, in which viscous forces were neglected, with just this side-force at $x = L$ taken into account. The resultant U_{cd} is reasonably close (for high enough f) to that given when considering the forces on the rest of the cylinder as well: e.g., for $f = 0{\cdot}8$, for end-force only, one obtains $\mathscr{U}_{cd} \simeq 1{\cdot}78$, and taking the forces on the rest of the body into account $\mathscr{U}_{cd} \simeq 2{\cdot}03$; indeed, the forces on the rest of the cylinder tend to stabilize the system for divergence.

One interesting observation that has been made in the discussion of experimental results is that the effect of form drag on divergence is destabilizing. This may be clarified by analogy to a taught string. The work done W in displacing the string a small distance $y(x)$ from equilibrium—cf. Morse (1948, p. 30)—is

$$W = -\tfrac{1}{2}\int_0^L y\frac{\mathrm{d}}{\mathrm{d}x}\left(T(x)\frac{\mathrm{d}y}{\mathrm{d}x}\right)\mathrm{d}x = -\tfrac{1}{2}\left[T(x)y\,\frac{\mathrm{d}y}{\mathrm{d}x}\right]_0^L + \frac{1}{2}\int_0^L T(x)\left(\frac{\mathrm{d}y}{\mathrm{d}x}\right)^2\mathrm{d}x.$$

If the string, or cylinder, is supported at both ends, the first term vanishes, while the second is always positive. If, however, there is a free end, and if y and $\mathrm{d}y/\mathrm{d}x$ have the same sign, then the first term may dominate, which would mean a negative-stiffness, destabilizing effect. As seen in Figures 3(a) and 4(a), y and $\mathrm{d}y/\mathrm{d}x$ do have the same sign. Hence, setting $T(L) = \frac{1}{2}\rho D^2 U^2 C_b$ shows that increasing the form drag may indeed be destabilizing; cf. the results in footnote 6 (Section 2.3.2).

3.2. The Mechanism of Flutter

Using equation (2) again, the rate of work done by the fluid on a cylinder with any boundary condition, in the course of free periodic motion, is

$$\begin{aligned}\frac{\mathrm{d}W}{\mathrm{d}t} = &-\int_0^L EI\,\dot{y}y''''\mathrm{d}x - \int_0^L \dot{y}M(\ddot{y} + 2U\,\dot{y}' + U^2\,y'')\,\mathrm{d}x + \int_0^L \dot{y}\{B - Fx\}y''\mathrm{d}x\\ &-\tfrac{1}{2}c_N\int_0^L (MU/D)\dot{y}(\dot{y} + Uy')\mathrm{d}x - \tfrac{1}{2}c^*\int_0^L (M/D)\dot{y}^2\,\mathrm{d}x - \int_0^L \dot{y}(m - \rho A)gy'\,\mathrm{d}x,\end{aligned}$$

where $c^* = (4/\pi)C_D$ with dimensions of velocity, and primes and overdots denote x- and t-derivatives, respectively; here $\{B - Fx\}$ stands for the expression in curly brackets in equation (2). Over a period of oscillation, T, the work done ΔW is

$$\begin{aligned}\Delta W = &-\int_0^T [\dot{y}\{EI\,y''' + MU(\dot{y} + U\,y')\}]_0^L\mathrm{d}t + \tfrac{1}{2}(1-\delta)M\,U^2\,c_b\int_0^T [\dot{y}y']_0^L\mathrm{d}t\\ &-\tfrac{1}{2}c_N(MU/D)\int_0^T\int_0^L (\dot{y}^2 + U\dot{y}y')\mathrm{d}x\,\mathrm{d}t + \tfrac{1}{2}\,c_T(MU^2/D)\int_0^T\int_0^L \dot{y}y'\mathrm{d}x\,\mathrm{d}t\\ &-\tfrac{1}{2}\,c^*\,(M/D)\int_0^T\int_0^L \dot{y}^2\mathrm{d}x\,\mathrm{d}t. \qquad (8)\end{aligned}$$

[7] See Jones (1945) and Hoerner (1985, p. 17.2), and refer to Katz & Plotkin (1991, Section 8.2).

To obtain this equation, extensive use of integration by parts has been made, while recalling that the oscillation is periodic. For instance,

$$\Delta W_{T^*} = \int_0^T \int_0^L \dot{y} T^* y'' \mathrm{d}x\,\mathrm{d}t = T^* \int_0^T [\dot{y}y']_0^L \mathrm{d}t - T^* \int_0^T \int_0^L \dot{y}' y' \,\mathrm{d}x\,\mathrm{d}t,$$

where $T^* \equiv B = \delta[\bar{T} + (1-2v)\bar{p}A] + \frac{1}{2}(1-\delta)MU^2 c_b$. The last integrand may be written as $\frac{1}{2}[(\partial/\partial t)(y')^2]$ and, since $y'^2|_{t=T} = y'^2|_{t=0}$ for all x, the second integral is zero. So is the first integral, for a system with both ends supported, since $\dot{y}(L) = \dot{y}(0) = 0$. However, for a cantilevered system ($\delta = 0$), we do have a contribution, namely $\frac{1}{2} MU^2 c_b \int_0^T \dot{y}_L y'_L \mathrm{d}t$.

Proceeding in a similar way with all the terms, for a cylinder supported upstream and free downstream, we have

$$\begin{aligned} \Delta W = & -(1-f)MU \int_0^T [\dot{y}^2 + U\dot{y}y']_L \mathrm{d}t + \tfrac{1}{2}MU^2 c_b \int_0^T [\dot{y}y']_L \mathrm{d}t \\ & - \tfrac{1}{2} c_N (MU/D) \int_0^T \int_0^L (\dot{y}^2 + U\dot{y}y') \,\mathrm{d}x\mathrm{d}t \\ & - \tfrac{1}{2}(M/D) \int_0^T \int_0^L \left(c^* \dot{y}^2 - c_T U^2 \dot{y}y'\right) \mathrm{d}x\,\mathrm{d}t, \end{aligned} \tag{9}$$

to obtain which we have made use of equation (3a) for $EI\, y'''|_{x=L}$, while neglecting the small terms involving s_e and $\bar{s}_e$. The first term on the right-hand side is associated with the inviscid forces, the second (involving c_b) with the base drag at the free end, and the third and fourth with frictional forces in the lateral direction (involving c_N and c^*) and the longitudinal direction (involving c_T)—cf. equations (2) and (3a), and the definitions of c_N, c_T and c_b in (5). This expression is a little different from those given before (Païdoussis 1966*a*, 1973), which are incomplete.

If $\Delta W < 0$, oscillations are damped by the flow, while for $\Delta W > 0$ oscillations are amplified, i.e. the system will be unstable by flutter.

Examining equation (9), it is clear that, unless $f = 1$, the dominant term controlling ΔW is the first. Indeed, apart from the $(1-f)$ factor, this term is identical to ΔW for internal flow [Païdoussis 1998, equation (3.11)]. Hence, the same observations and conclusions may be reached albeit modified by viscous effects; e.g. the requirement that $\overline{y'(L,t)\dot{y}(L,t)} < 0$ over a cycle must be satisfied for energy transfer from the fluid to the cylinder, which means that over most of the cycle the free end of the cylinder slopes backwards to the direction of motion, exactly as observed in experiments.

One important difference *vis-à-vis* the internal flow system is the existence of the second term in equation (9), especially since (i) it works in opposition to the first term, and (ii) we normally peg c_b on f : $c_b = 1 - f$. This is discussed at the end of this subsection.

Equation (9) also shows that if $f = 1$, the inviscid first term vanishes, i.e. the work done by the nonviscous nonconservative forces vanishes. This signifies that the main source of energy transfer from the fluid to the solid ceases to exist, though energy exchange may still occur via the viscous forces; indeed, apart from the viscous forces, the system becomes like a conservative one. Significantly, this also coincides with the suppression of single-mode flutter and its replacement by coupled-mode flutter [see Part 3; also, compare with the dynamics of pipes conveying fluid (Païdoussis 1998, Section 3.4.1)].

The last item of interest is what happens when $f \to 0$. According to equation (9), the system would then be more strongly nonconservative for $f = 0$ than for any other f; yet, it has been found that flutter with a blunt end does not occur.

TABLE 3

The effect of c_b and εc_f on flutter for $f = 0$, $\beta = 0{\cdot}47$, $c_N = c_T = c_f$

c_b	$\mathscr{U}_{cf}$ ($\varepsilon c_f = 0$)	$\mathscr{U}_{cf}$ ($\varepsilon c_f = 0{\cdot}25$)	$\mathscr{U}_{cf}$ ($\varepsilon c_f = 1{\cdot}0$)
0	9·13	9·72	14·9
1	28·1	36·9	—*
2	—	—	—

*See comments in the text; if $\mathscr{U}_{cf}$ exists in this case, it is very high.

In fact, flutter *is* possible for $f = 0$, *provided that*, artificially, $c_b = 0$. This is made clear by the results in Table 3. Even for $c_b = 1$, flutter is possible, but at flow velocities beyond the range of the experiments reported here.[8] For $\varepsilon c_f = 1$ and $c_b = 1$, the critical value could not be pin-pointed, beyond stating that $\mathscr{U}_{cf} > 40$, if it exists at all, since results for such high $\mathscr{U}$ are very sensitive to the number of comparison functions, N, used in the calculation; in fact, calculations with increasing N suggest that perhaps $\mathscr{U}_{cf} \to \infty$ in this case.

For $c_b = 2$, however, no flutter is possible with $f = 0$. As may be seen from equation (9), the components of the first two terms involving $(\dot{y}y')_L$ cancel each other out. Although the possibility of flutter via the viscous terms involving c_N, c_T and c^* exists, it was found not to materialize in the calculations.

Hence, it may be concluded that, for very blunt ends, (i) divergence disappears because f becomes too small, and (ii) flutter disappears because c_b becomes too large.

4. DISCUSSION AND CONCLUSION

In this paper, experiments with cantilevered cylinders in essentially unconfined flow have been described: (i) for completeness, some earlier experiments (1966) in which the cylinders were horizontal, and (ii) a recently conducted set (1999–2000), involving vertical cylinders. In the former set, in most cases, the cylinders were fitted with a thin metal blade in their central plane, to ensure planar motion in a horizontal plane. In the latter, again in most cases, there was no such constraining blade.

The dynamical behaviour was, in one sense, the same in both cases. Initially, as the flow was increased, flow-induced damping was generated, but small vibration could be observed in which the cylinder responded to the turbulence-induced fluctuating pressure field. At higher flow velocities, the system developed divergence in its first mode, then regained its equilibrium configuration (more or less), before developing flutter spontaneously in its second mode. As the flow velocity continued to increase, second-mode flutter was succeeded by third-mode flutter, and in some cases fourth-mode flutter. This was the dynamical behaviour for a cylinder with a reasonably well-streamlined ogival end-shape at the free end. If, however, the end was completely blunt, then neither static (divergence) or dynamic (flutter) instabilities materialized.

In another sense, however, the dynamics in cases when there was no metal strip (blade) embedded in the cylinder, whether vertical or horizontal, was profoundly different, at least so far as flutter is concerned. In that case, instead of being planar, the flutter involved an orbital, "whirling" mode-shape. Nevertheless, the critical flow velocities, to the extent that this could be ascertained, were not substantially altered.

[8] The maximum attainable in the early experiments (horizontal system) was $\mathscr{U} \simeq 14$, while in the more recent set $\mathscr{U} \simeq 8$.

Some of these results have been compared with those obtained by linear theory (Part 3 of this work) and agreement has been found to be reasonable, though certainly not brilliant.

Then, in Section 3 of this paper, a synthesis of experimental observations and energy considerations from the equations of motion (without solving them) permitted us to draw some general conclusions about the mechanisms of instabilities at the physical level.

Thus, it has been found that divergence is principally dependent on the presence of the tapering end, specifically on having a free-end shape such that $\mathrm{d}A/\mathrm{d}x \neq 0$, A being the cross-sectional area. This was linked to the dynamics of low aspect-ratio wings. This being an inherently nonconservative system, one should not be surprised by unusual or paradoxical behaviour—cf. Païdoussis (1998). One such characteristic is that added drag at the free end of the cylinder *destabilizes* the system for divergence.

The situation for flutter is more complex and more interesting. In this case, the system is stabilized as the free-end shape becomes blunter, yet at the same time it becomes more capable of extracting energy from the fluid (i.e., it becomes more strongly nonconservative)—as characterized by a decrease in the streamlining parameter f. It is shown in Section 3.2 that, in principle, flutter could occur for a blunt downstream end, if only the naturally occurring form (base) drag at the free end could be suppressed. For flutter, increased drag at the free end stabilizes the system.

A number of other, more general conclusions on the dynamics of this system, especially on the nonlinear dynamics, are presented in Part 3 of this work, where the main theoretical results are presented (Semler *et al*. 2002).

ACKNOWLEDGEMENTS

The authors gratefully acknowledge the support received from the Natural Sciences and Engineering Research Council of Canada and Le Fonds FCAR of Québec.

REFERENCES

Bejan, A. 1982 The meandering fall of paper ribbons. *Physics of Fluids* **25,** 741–742.

Chang, Y. B. & Moretti, P.M. 2000 Flow-induced vibration of free edges of thin films. In *Flow-Induced Vibration* (eds S. Ziada & T. Staubli), pp. 801–810. Rotterdam: A.A. Balkema.

Chen, S. S. 1975 Vibration of nuclear fuel bundles. *Nuclear Engineering and Design* **35,** 399–422.

Dowling, A. P. 1988*a* The dynamics of towed flexible cylinders. Part 1: neutrally buoyant elements. *Journal of Fluid Mechanics* **187,** 507–532.

Dowling, A. P. 1988*b* The dynamics of towed flexible cylinders. Part 2: negatively buoyant elements. *Journal of Fluid Mechanics* **187,** 533–571.

Gagnon, J. O. & Païdoussis, M. P. 1994*a* Fluid coupling characteristics and vibration of cylinder clusters in axial flow. Part I: theory. *Journal of Fluids and Structures* **8,** 257–291.

Gagnon, J. O. & Païdoussis, M. P. 1994*b* Fluid coupling characteristics and vibration of cylinder clusters in axial flow. Part II: experiments. *Journal of Fluids and Structures* **8,** 293–324.

Hannoyer, M. J. & Païdoussis, M. P. 1978 Instabilities of tubular beams simultaneously subjected to internal and external axial flows. *ASME Journal of Mechanical Design* **100,** 328–336.

Hawthorne, W. R. 1961 The early development of the Dracone flexible barge. *Proceedings of the Institution of Mechanical Engineers* **175,** 52–83.

Hoerner, S. F. 1985 *Fluid Dynamic Lift*. Albuquerque: Hoerner Fluid Dynamics.

Holmes, P. J. 1977 Bifurcations to divergence and flutter in flow-induced oscillations: a finite-dimensional analysis. *Journal of Sound and Vibration* **53,** 471-503.

Holmes, P. J. 1978 Pipes supported at both ends cannot flutter. *Journal of Applied Mechanics* **45,** 619–622.

JONES, R. T. 1945 Properties of low-aspect ratio pointed wings at speeds below and above the speed of sound. NACA Report 835.

KATZ, J. & PLOTKIN, A. 1991 *Low-Speed Aerodynamics: from Wing Theory to Panel Methods*. New York: McGraw-Hill.

LOPES, J.-L., PAÏDOUSSIS, M. P. & SEMLER, C. 2002 Linear and nonlinear dynamics of cantilevered cylinders in axial flow. Part 2: The equations of motion. *Journal of Fluids and Structures* **16,** 715–737.

MATEESCU, D., PAÏDOUSSIS, M. P. & BÉLANGER, F., 1994*a* Unsteady annular viscous flows between oscillating cylinders. Part I: computational solutions based on a time-integration method. *Journal of Fluids and Structures* **8,** 489–507.

MATEESCU, D., PAÏDOUSSIS, M. P. & BÉLANGER, F., 1994*b* Unsteady annular viscous flows between oscillating cylinders. Part II: a hybrid time-integration solution based on azimuthal Fourier expansions for configurations with annular backsteps. *Journal of Fluids and Structures* **8,** 509–527.

MATEESCU, D., MEKANIK, A. & PAÏDOUSIS, M. P. 1996 Analysis of 2-D and 3-D unsteady annular flows with oscillating boundaries, based on a time-dependent coordinate transformation. *Journal of Fluids and Structures* **10**, 57–77.

MORSE, P. M. 1948 *Vibration and Sound*, 2nd edition. New York: McGraw Hill; American Institute of Physics (1976).

MOTE Jr, C. D. 1968 Dynamic stability of an axially moving band. *Journal of the Franklin Institute* **285,** 329–346.

MOTE Jr, C. D. 1972 Dynamic stability of axially moving material. *Shock and Vibration Digest* **14**(4), 2–11.

ORTLOFF, C. R. & IVES, J. 1969 On the dynamic motion of a thin flexible cylinder in a viscous stream. *Journal of Fluid Mechanics* **38,** 713–720.

PAÏDOUSSIS, M. P. 1966*a* Dynamics of flexible slender cylinders in axial flow. Part 1: theory. *Journal of Fluid Mechanics* **26,** 717–736.

PAÏDOUSSIS, M. P. 1966*b* Dynamics of flexible slender cylinders in axial flow. Part 2: experiments. *Journal of Fluid Mechanics* **26,** 737–751.

PAÏDOUSSIS, M. P. 1968 Stability of towed, totally submerged flexible cylinders. *Journal of Fluid Mechanics* **34,** 273–297.

PAÏDOUSSIS, M. P. 1970 Dynamics of submerged towed cylinders. *Eighth Symposium on Naval Hydrodynamics: Hydrodynamics in the Ocean Environment*. Office of Naval Research, U.S. Department of the Navy ARC-179, pp. 981–1016.

PAÏDOUSSIS, M. P. 1973 Dynamics of cylindrical structures subjected to axial flow. *Journal of Sound and Vibration* **29,** 365–385.

PAÏDOUSSIS, M. P. 1979 The dynamics of clusters of flexible cylinders in axial flow: theory and experiments. *Journal of Sound and Vibration* **65,** 391–417.

PAÏDOUSSIS, M. P. 1993 *Calvin Rice Lecture*: Some curiosity-driven research in fluid–structure interactions and its current applications. *ASME Journal of Pressure Vessel Technology* **115,** 2–14.

PAÏDOUSSIS, M. P. 1998 *Fluid–Structure Interactions: Slender Structures and Axial Flow*, Vol. 1. London: Academic Press.

PAÏDOUSSIS, M. P. 2002 *Fluid–Structure Interactions: Slender Structures and Axial Flow*, Vol. 2. London: Academic Press.

PAÏDOUSSIS, M. P. & YU, B. K., 1976 Elastohydrodynamics and stability of towed slender bodies of revolution. *AIAA Journal of Hydronautics* **10,** 127–134.

PAÏDOUSSIS, M. P., MATEESCU, D. & SIM, W.-G. 1990 Dynamics and stability of a flexible cylinder in a narrow coaxial cylindrical duct subjected to annular flow. *Journal of Applied Mechanics* **57,** 232–240.

PRAMILA, A. 1986 Sheet flutter and the interaction between sheet and air. *TAPPI Journal* **69,** 70–74.

PRAMILA, A. 1987 Natural frequencies of a submerged axially moving band. *Journal of Sound and Vibration* **113,** 198–203.

SEMLER, C., LOPES, J.-L., AUGU, N. & PAÏDOUSSIS, M. P. 2002 Linear and nonlinear dynamics of cantilevered cylinders in axial flow. Part 3: nonlinear dynamics. *Journal of Fluids and Structures* **16,** 739–759.

TRIANTAFYLLOU, G. S. & CHRYSSOSTOMIDIS, C. 1984 Analytic determination of the buckling speed of towed slender cylindrical beams. *ASME Journal of Energy Resources Technology* **106,** 246–249.

TRIANTAFYLLOU, G. S. & CHRYSSOSTOMIDIS, C. 1985 Stability of a string in axial flow. *ASME Journal of Energy Resources Technology* **107,** 421–425.

TRIANTAFYLLOU, G. S. & CHRYSSOSTOMIDIS, C. 1989 The dynamics of towed arrays. *ASME Journal of Offshore Mechanics and Arctic Engineering* **111,** 208–213.

TRIANTAFYLLOU, M. S. 1998 Private communication.

WICKERT, J. A. & MOTE Jr, C. D., 1990 Classical vibration analysis of axially moving continua. *Journal of Applied Mechanics* **57,** 738–744.